ENTHESIS: NOT THE SAME IN EACH LOCALISATION – A MOLECULAR, HISTOLOGICAL AND BIOMECHANICAL STUDY

C.J. Peniche Silva[1,§], S.A. Müller[2,3,§], N. Quirk[2], R.E. De la Vega[1,2], M.J. Coenen[2], C.H. Evans[2], E.R. Balmayor[2,4] and M. van Griensven[1,2,*]

[1] cBITE, MERLN Institute for Technology-Inspired Regenerative Medicine, Maastricht University, Maastricht, the Netherlands
[2] Musculoskeletal Gene Therapy Laboratory, Rehabilitation Medicine Research Center, Mayo Clinic, Rochester, MN, USA
[3] Medizinische Fakultät, University of Basel, Basel, Switzerland
[4] Department of Orthopaedic, Trauma and Reconstructive Surgery, RWTH Aachen University Hospital, Aachen, Germany
[§] These authors contributed equally to this work

Abstract

The interphase between tendon and bone consists of a highly specialised tissue called enthesis. Typically, the enthesis is described as a succession of four different zones: tendon, non-mineralised fibrocartilage, mineralised fibrocartilage and bone. However, the microstructure of the entheses, cellular composition and mechanical properties vary depending on their anatomical location. The present study aimed to characterise three of the most relevant sites of enthesis injury in a rat model: the patellar tendon, the Achilles tendon and the supraspinatus enthesis, in terms of biomechanics, histology and genetic expression. The patellar enthesis presented the highest ultimate load and lowest stiffness of the three, while the supraspinatus was the weakest and stiffest. The histological characterisation revealed key differences at the insertion site for each enthesis. The patellar enthesis showed a large cartilaginous area at the tendon-to-bone interphase whilst this interphase was smaller in the supraspinatus entheses samples. Furthermore, the Achilles tendon enthesis displayed a more abrupt transition from tendon to bone. Additionally, each enthesis exhibited a particular and distinct pattern of expression of tenogenic, chondrogenic and osteogenic markers. This study provided valuable insights for a better understanding of the three entheses at relevant anatomical sites. Moreover, the larger cross-sectional area of the patellar enthesis, the strong mechanical properties and the easier surgical access to this location led to the conclusion that the patellar tendon enthesis site could be most suitable for the development of a preclinical model for general enthesis regeneration studies in rats.

Keywords: Enthesis, patellar tendon, Achilles tendon, supraspinatus.

***Address for correspondence**: Prof. Dr Martijn van Griensven, Chair Department cBITE, MERLN Institute, Maastricht University, Universiteitssingel 40, 6229 ER Maastricht, the Netherlands.
Telephone number: +31 646705565 Email: m.vangriensven@maastrichtuniversity.nl

Copyright policy: This article is distributed in accordance with Creative Commons Attribution Licence (http://creativecommons.org/licenses/by/4.0/).

List of Abbreviations

ANOVA	analysis of variance
BSA	bovine serum albumin
Col1a1	collagen type I alpha 1 chain
Col2a1	collagen type II alpha 1 chain
Col3a1	collagen type III alpha 1 chain
Col10	ca1collagen type X alpha 1 chain
Ct	cycle threshold
DAPI	4′,6-diamidino-2-phenylindole
EDTA	ethylenediaminetetraacetic acid
Fn1	fibronectin 1
H&E	haematoxylin and eosin
IHC	immunohistochemistry
Mkx	Mohawk homeobox
PBS	phosphate-buffered Saline
ROI	region of interest
RT-PCR	real-time quantitative reverse transcription polymerase chain reaction
Runx2	Runt-related transcription factor 2
Sox9	SRY-Box transcription factor 9

Sparc	secreted protein acidic and cysteine rich
Tnmd	tenomodulin

Introduction

Tendon attaches to bone through a highly specialised tissue called enthesis (Apostolakos *et al.*, 2014; Benjamin *et al.*, 2002). The microscopical and macroscopical structures of the enthesis, its cellular composition as well as the mechanical properties vary depending on the anatomical location to meet the mechanical demands at each insertion site (Killian, 2021). Generally, the entheses can be classified as fibrous or fibrocartilaginous (Benjamin *et al.*, 2000; 2002; 2006). The fibrous entheses are common in tendons that attach directly to the bone or the bone's periosteum, such as the deltoid attachment to the humerus and the *adductur magnus* to the *linea aspera* of the femur (Apostolakos *et al.*, 2014). Fibrocartilaginous entheses are more frequently found attaching tendons to long bone's epiphyses or apophyses and are normally present at high-stress concentration sites associated with joint movement (Benjamin *et al.*, 2000).

The majority of the entheses in the body are fibrocartilaginous entheses (Benjamin *et al.*, 2000; 2006). Among these, the supraspinatus, the Achilles tendon and the patellar tendon are considered some of the most frequent sites of enthesis injury due to acute trauma and/or tissue degeneration (Derwin *et al.*, 2018). Regrettably, torn or injured entheses often require surgery and its outcome is far from ideal, with high rupture recurrence rates and long-term complaints from the patients' side (Calejo *et al.*, 2019; Derwin *et al.*, 2018). This occurs mostly because of the complexity of the fibrocartilaginous structure of the tendon-to-bone enthesis and the intricacy of entheses' pathologies (Calejo *et al.*, 2019; Rossetti *et al.*, 2017; Watad *et al.*, 2018). Additionally, the wide range of factors influencing the healing process of the different entheses varies from one anatomical location to the other, as the risk factors and biology of the entheses are unique to the particular anatomical location (Calejo *et al.*, 2019; Derwin *et al.*, 2018; Paxton *et al.*, 2012).

Important breakthroughs have been achieved in recent years by tissue engineers working on novel therapies to improve the healing of the tendon-to-bone entheses (Bunker *et al.*, 2014; Font Tellado *et al.*, 2018; Nowlin *et al.*, 2018; Su *et al.*, 2019; Wang *et al.*, 2021). Most of these studies rely on the use of scaffolds or sponges combined with growth factors to promote the regeneration of the enthesis fibrocartilage zone (Font Tellado *et al.*, 2017; Nowlin *et al.*, 2018; Zhao *et al.*, 2020). Others, with limited success, have focused on the use of autografts and autologous periosteal flaps to regenerate the cartilaginous tendon-to-bone transition zone (Holwein *et al.*, 2019; Lee *et al.*, 2017; Novakova *et al.*, 2018). However, despite the efforts, the challenges still to overcome are many. They range from the lack of understanding of the development and healing mechanisms of the entheses to the need for a relevant animal model for the translation of novel treatments (Derwin *et al.*, 2018).

The use of experimental animals is an unfortunate yet necessary, phase in current biomedical research (Baumans, 2004). For many years, tissue engineers working on musculoskeletal regeneration have trusted animal-based research to learn, develop and validate new concepts and novel therapies (Fan *et al.*, 2020; Novakova *et al.*, 2018; Rothrauff *et al.*, 2019; Wang *et al.*, 2021). Moreover, enthesis-related research not only exploits different animal models but also focuses on different anatomical locations (Fu *et al.*, 2018; Sun *et al.*, 2020; Zhang *et al.*, 2018), which makes the translation of the developed therapies somewhat difficult. This is why the establishment of a suitable animal model for entheses regeneration studies is of utmost importance to improve the quality of entheses research and the translation of new findings.

Focusing on this challenge, the present study aimed at the characterisation in a rat model of the 3 most relevant sites of enthesis injury (*i.e.* patellar tendon, Achilles tendon and supraspinatus) in terms of biomechanics, histology and gene expression, to gain an overall knowledge. This may help in the future to select one as the ultimate model for basic enthesis regeneration studies.

Materials and Methods

Collection of explants

10 male Sprague Dawley rats (Charles River Laboratories) weighing between 400 and 500 g (100-130 d old) were used. The animals were sacrificed for reasons unrelated to the present study while being in other studies that did not influence the enthesis.

After having received the sacrificed animals, sets of two samples of native (healthy) tendon-to-bone entheses from the patellar tendon, Achilles tendon and supraspinatus tendon per rat were harvested, for a total of 20 samples from each location. The patellar enthesis sample included the patellar tendon and its insertion site at the tibia. The Achilles tendon-to-bone enthesis samples were harvested as a muscle-tendon unit containing the Achilles tendon and its insertion site into the calcaneus. Similarly, the supraspinatus samples comprised the supraspinatus tendon-muscle unit and its insertion site at the head of the humerus.

Biomechanical measurements and testing

Samples to be used for mechanical testing ($n = 12$ per location) were wrapped in a gauze soaked with saline and stored in a 15 mL Falcon tube at − 20 °C until the day of testing (Quirk *et al.*, 2018).

Before the testing, samples were thawed for 4 h at room temperature while kept moist using saline. Afterward, the tendon length of each sample, from

the tendon origin at the muscle to the enthesis and the enthesis cross-sectional area (width × depth) were measured using an electronic Vernier calliper (CD-8 ASX, Mitutoyo, Kawasaki, Japan).

For the mechanical testing, a custom-made small biological specimen mechanical-testing machine (Mayo Clinic, Rochester, MN, USA) with a 222.4 N loadcell limit (MLP-2, Transducer Techniques, Temecula, CA, USA) and associated LabVIEW 2017 SP1 (National Instruments, Austin, TX, USA) was employed. Custom-made mounting fixtures were previously developed similarly to other reported tissue-testing clamps (Wieloch *et al.*, 2004). Samples from the Achilles tendon were tested through isolation of the calcaneus and ensuring the correct orientation of the tendon by utilising a custom-made foot support. The entheses samples from the patellar tendon and supraspinatus tendon were tested through clamping of the tibia and humerus respectively, allowing the alignment of the tendon. Custom-built cryo-clamps were used in conjunction with dry-ice powder to secure sample muscle attachments proximally (Fig. 1**d.1**,**d.2**).

During the freezing period, the temperature of the entheses as well as of the proximal and middle tendons was monitored utilising a TrueRMS multi-meter (TrueRMS Supermeter, Newport, RI, USA) to ensure optimal fixation. The optimal temperature for enthesis testing was determined in a previous study (Quirk *et al.*, 2018). A mean temperature of − 1 °C at the proximal tendon region assured sufficient muscle freezing to prevent the muscle to slip from the clamps. All samples were tested at a mean temperature of 10 °C at the enthesis region, which ensured that the testing could be performed reproducibly while the samples were not frozen. Samples were preloaded to 3 N prior to 200 mm/min failure tensile test (Quirk *et al.*, 2018). During the mechanical testing, enthesis tears were monitored in real-time by a consistent single operator throughout. No tears occurred in the tendon or the bony part of any of the specimens tested for each group.

Force-elongation curves were recorded, from which ultimate load (force at failure; N), stiffness (loading curve linear portion; N/mm) and tangent modulus (force at failure/enthesis cross-sectional area/ultimate strain; MPa) were calculated. Data were processed individually using Matlab 2016a (Mathworks), compiled in Microsoft Excel 2010 (Microsoft) and statistically assessed using GraphPad Prism 8.0 (GraphPad Software). Measurable data and calculated mechanical property data are reported through box plots (median, 1st, 3rd quartile ranges and outliers boundaries at 10-90 percentile).

Histology and IHC

Samples from the 3 entheses ($n = 8$ per location) were fixed in 4 % paraformaldehyde (Sigma-Aldrich) for 48 h, rinsed in PBS and decalcified in 10 % buffered EDTA (Sigma-Aldrich) for 28 d. Buffer was exchanged every 2 to 3 d and the endpoint of the decalcification was determined by macroscopical inspection. For this, the tissue samples were inspected every 5 d by gently compressing their bony area by hand until a gel-like consistency was attained from all angles. After reaching the point where no sharp edges or

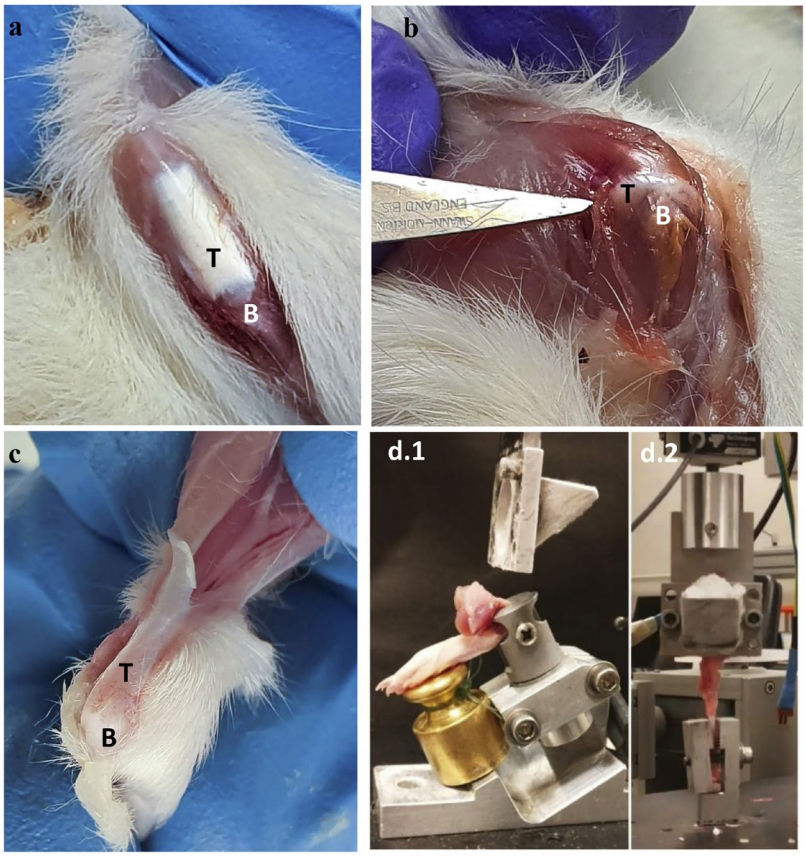


Fig. 1. Representative images of the exposed entheses. (**a**) Patellar enthesis with associated tendon. (**b**) Achilles enthesis with associated tendon. (**c**) Supraspinatus enthesis with associated tendon. T and B indicate tendon and bone tissues at their respective sides of the enthesis. (**d**) Custom-made mechanical testing fixtures. (**d.1**) Achilles enthesis fixture. Calf muscle is not yet mounted to cryo-clamp. (**d.2**) Patellar and supraspinatus testing set-up.

Table 1. List of the antibodies and working dilution used for IHC.

Name	Abcam ID number	Working dilution
Anti-collagen type I	ab270993	1:250
Anti-collagen type II	ab34712	1:50
Anti-collagen type III	ab6310	1:250
Anti-collagen type X	ab49945	1:100
Rabbit IgG isotype control	ab172730	1:50
Mouse IgM isotype control	ab18401	1:100
Mouse IgG1 isotype control	ab170190	1:250
Alexa Fluor 647 goat anti-rabbit	ab190565	1:500
Alexa Fluor 647 goat anti-mouse	ab15015	1:500

hard tissue were perceived by compression, 1 sample was selected, cut using a scalpel and thoroughly inspected to confirm that the decalcification endpoint was attained. After decalcification, samples were dehydrated in an ethanol series (50 %, 70 %, 96 % and 100 %) and embedded in paraffin-wax. Longitudinal cross-sections were sliced at a thickness of 7 μm using a Leica RM 2165 microtome (Leica Biosystems). Afterward, H&E, safranin O, toluidine blue and picrosirius red stainings were performed.

Briefly, samples were dewaxed in NeoClear-xylene substitute (Merck KGaA) and rehydrated in a descending ethanol series (100 %, 96 %, 70 % and 50 %) and distilled water. For the H&E staining, samples were incubated with haematoxylin solution for 10 min and eosin for 2 min (Carl Roth GmbH), dehydrated in an ascending ethanol series (70 %, 96 % and 100 %), cleared using NeoClear-xylene substitute (Merck KGaA) and mounted using UltraKit mounting media (Thermo Fisher Scientific). The toluidine blue staining was performed by incubating the rehydrated slides in a working solution of toluidine blue (0.1 % toluidine blue, pH 2.5, Sigma-Aldrich) for 3 min, followed by 3 washes with distilled water. Subsequently, the slides were dehydrated in an ascending ethanol series (%?), cleared using NeoClear-xylene substitute and mounted using UltraKit mounting media.

For the safranin O staining, the rehydrated slides were stained with haematoxylin solution for 10 min, followed by 5 min staining with 0.1 % fast green solution (Sigma-Aldrich), rinsed with 0.1 % acetic acid and further stained with 0.1 % safranin O solution for 10 min (Sigma-Aldrich). Subsequently, the samples were dehydrated, cleared and mounted as described before. The stained slides were imaged using a Nikon DS-Ri2 camera mounted on a Nikon Ti Slide Scanner Microscope.

The picrosirius red staining was conducted on slides that were previously rehydrated and stained with haematoxylin solution for 10 min. Incubation with 0.1 % picrosirius red working solution (Sigma-Aldrich) was done for 1 h followed by 2 washes with acidified water. Later, the samples were dehydrated, cleared and mounted as previously described. Imaging was done using an inverted Nikon Ti-S/L100 microscope.

As part of the histological characterisation, the orientation angle of the collagen fibres at the tendon-to-bone interphase of the enthesis was measured in the picrosirius-red-stained samples using Image J v1.53p (NIH). For this, the images of the stained samples were rotated to match the same orientation using the bony site of the entheses as the reference to set the horizontal line. Afterward, 3 different ROIs were set at the tendon-to-bone interphase, ROI1 at the left end of the interphase, ROI2 at the middle portion of the cross-section and ROI3 at the right end of the interphase. The orientation angle of each ROI was measured using the Image J plugin Orientation J_Measure-v2.0.4. The values were imported to Microsoft Excel 2016 (Microsoft) and the variability of the orientation angle among the 3 ROIs was calculated for each anatomical location.

For the IHC, all primary and secondary antibodies (Table 1), as well as the DAPI (ab285390) staining solutions were purchased from Abcam. Antigen retrieval was performed on the rehydrated samples by incubation in 10 mmol/L citrate buffer (pH 6) for 10 min at 95 °C followed by blocking with 1 % BSA (Sigma-Aldrich) for 1 h at room temperature. Afterward, the slides were placed in a humidity chamber and incubated overnight at 4 °C with the primary antibody diluted in blocking solution, followed by incubation with the secondary antibody for 2 h at room temperature. Finally, counterstaining with DAPI was performed and the slides were mounted using Dako fluorescent mounting media (Agilent Technology).

The stained slides were imaged using a Nikon DS-Ri2 camera mounted on a Nikon Ti Slide Scanner Microscope.

Gene expression

Immediately after the mechanical testing, the muscle-tendon unit and bony portions of the tissue samples were separated from the entheses, leaving only the respective tendon-to-bone insertion site at the bony end of the entheses (n = 12). Then, the entheses samples were homogenised using stainless-steel beads in the presence of TRIzolTM reagent (Thermo Scientific) using a Qiagen TissueLyser LT set at 50 Hz for periods of 5 min following a step of snap-freeze using liquid nitrogen.

Table 2. Primers used for RT-PCRs.

Target	Forward 5′→3′	Reverse 5′→3′
Col1a1	TTTCCCCCAACCCTGGAAAC	CAGTGGGCAGAAAGGGACTT
Col2a1	CACGCCTTCCCATTGTTGAC	AGATAGTTCCTGTCTCCGCCT
Col3a1	TGCAATGTGGGACCTGGTTT	GGGCAGTCTAGTGGCTCATC
Col10a1	TCCCAGGATTCCCTGGATCTAA	TACCGCTGGGTAAGCTTTGG
Mkx	GACGACGGCTGAAGAACACTG	CCTCTTCGTTCATGTGAGTTCTTGG
Tnmd	GTCCCACAAGTGAAGGTGGA	TTGCAAGGCATGATGACACG
Scx	GACCGCACCAACAGCGTGAA	GTGGACCCTCCTCCTTCTAACTTC
Fn1	CCCCAACTGGTTACCCTTCC	TGGTTCGCCTAAAGCCATGT
Sparc	CCTCAGACGGAAGCTGCAGAA	ACCAGGACGTTTTTGAGCCA
Runx2	CAAGGAGGCCCTGGTGTTTA	AAGAGGCTGTTTGACGCCAT
Sox9	CCTCCTACCCAACCATCACG	GAGCTGTGTGTAGACGGGTT
β-tubulin	GAGGGCGAGGACGAGGCTTA	TCTAACAGAGGCAAAACTGAGCACC

The extraction of the total RNA was performed following the well-established phenol/chloroform extraction protocol. The final concentration and purity of the obtained total RNA were measured using a BioDrop μLite UV/Vis spectrophotometer (BioDrop, Cambridge, UK). The cut-off value for RNA purity (ratios A260/230 and 260/280) was set at 2.0. All the samples yielded values of A260/230 and 260/280 ratios between 2.0 and 2.2.

The extracted RNA was the starting material for the cDNA synthesis. The cDNA synthesis was performed using a PeqLab Thermocycler (AvantorTM, Radnor, PA, USA) and the iScript cDNA synthesis kit (Bio-Rad Laboratories) following the manufacturer's instructions. The reaction mix was prepared using 10 μL of RNA template (250 ng), 4 μL of 5× iScript Reaction Mix, 1 μL of iScript Reverse transcription mix and 5 μL of ultra-pure nuclease-free water, for a total volume of 20 μL per reaction. Then, the reaction mix was incubated at 25 °C for 5 min, followed by 46 °C for 20 min and 95 °C for 1 min.

The gene expression of a selection of tenogenic, chondrogenic and osteogenic markers (Table 2) was analysed by single SYBR green-based RT-PCRs. The RT-PCR reactions were performed using a CFX96 Real-Time System Thermocycler (Bio-Rad Laboratoriey). For the RT-PCR reactions, 4 μL of cDNA template (5 ng) was added to the master mix containing 10 μL of iQTM SYBER® Green Supermix (Bio-Rad Laboratories), 2 μL of forward primer, 2 μL of reverse primer (300 mmol/L) and 2 μL of ultra-pure water, for a reaction volume of 20 μL. PCR amplification was conducted by using the following program: 90 °C for 3 min and 40 cycles of 95 °C for 10 s, 55 °C for 30 s and 95 °C for 30 s. A melting curve was performed at the end of the last amplification cycle. For the analysis of the results, Ct values higher than 35 were considered unreliable and, therefore, not included in the calculations of relative gene expression. Ct values ≤ 35 were exported to Microsoft Excel 2016 (Microsoft) and the ratio of expression between reference and target gene was calculated as $2^{(-\Delta Ct)}$ where ΔCt was calculated as Ct gene of interest − Ct reference gene. The statistical analysis of the gene expression was performed on the ΔCt values and assessed by GraphPad Prism 8.0 (GraphPad Software). The normalised gene expression data are reported as dot blots indicating mean and standard deviation of the ratio of expression $2^{(-\Delta Ct)}$.

β-tubulin was selected as the housekeeping gene by the ΔCt method for reference genes (Silver *et al.*, 2006). This method allows comparing the relative expression of pairs of genes within each sample to identify useful housekeeping genes. For this, β-actin, β2-microglobulin, lactate dehydrogenase A, ribosomal protein stalk subunit P1 and β-tubulin were compared. As a result of this comparison, β-tubulin was the highest scoring gene and, thus, the one with the most stable expression among the analysed samples.

Statistical analysis

Statistical analysis was performed using GraphPad Prism 8.0 (GraphPad Software). Data were tested for normal distribution by the D'Agostino & Person and Shapiro-Wilk normality test. Since the data were normally distributed in all cases, statistically significant differences were determined by one-way ANOVA with Tukey's multiple comparison test ($p < 0.05$).

Results

Mechanical testing

Before biomechanical characterisation, the length of the tendons of each enthesis and the entheses' cross-sectional area were measured (Fig. 2**a**,**b**). On the one hand, the patellar tendon was significantly longer ($p < 0.001$) than the supraspinatus tendon, while the Achilles tendon was the longest ($p < 0.001$). On the other hand, the cross-sectional area at the bony insertion site of the patellar enthesis resulted to be the largest ($p < 0.001$), with the Achilles and supraspinatus displaying less than half of the patellar enthesis cross-sectional area (Fig. 2**a**,**b**).

The biomechanical testing revealed that the measured ultimate load (Fig. 2**c**) was similar in

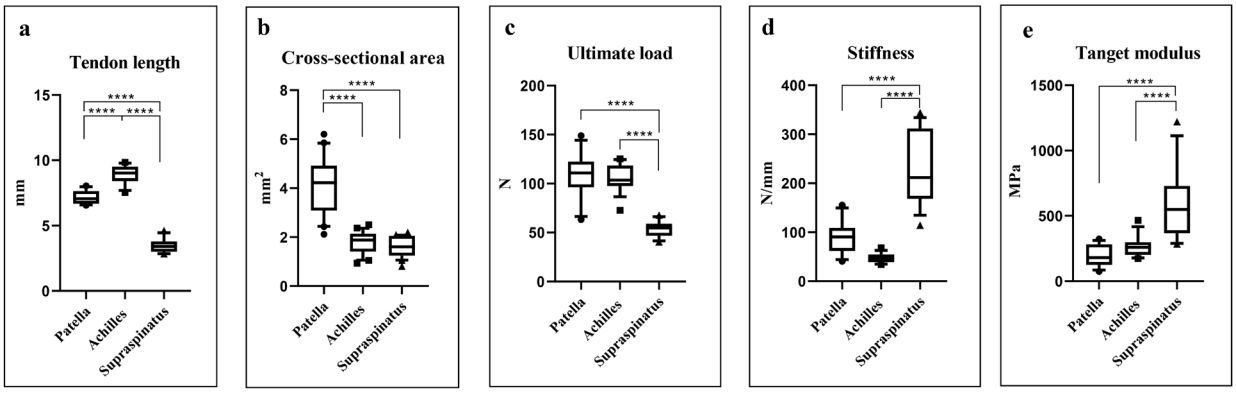


Fig. 2. Measurements and biomechanics of the 3 native entheses. (**a**) Tendon length, (**b**) cross-sectional area, (**c**) ultimate load, (**d**) stiffness, (**e**) tangent modulus. **** $p < 0.0001$.

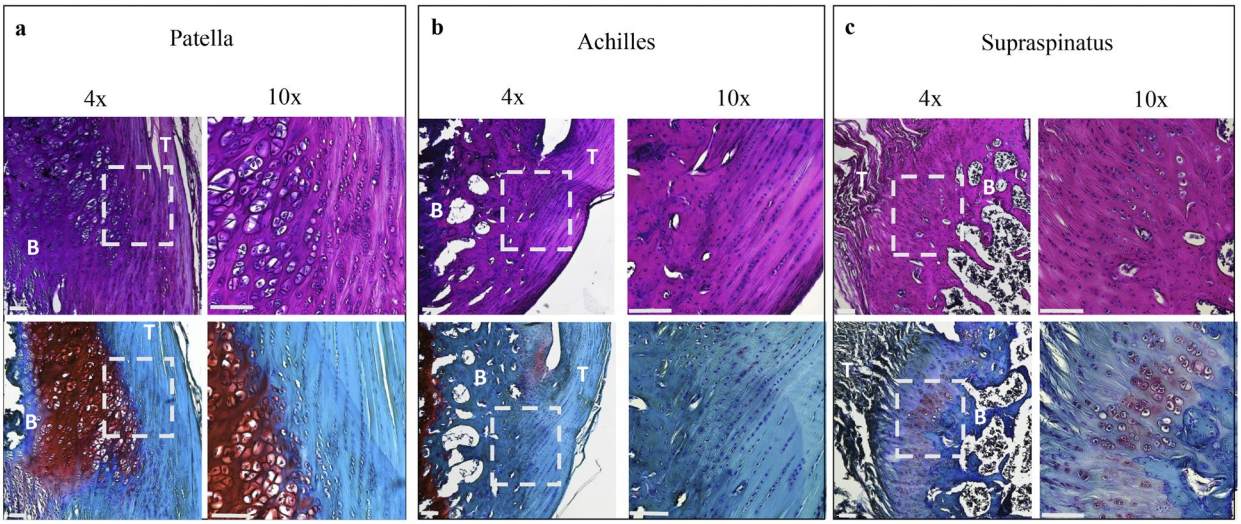


Fig.3. Histological staining of native entheses. (**a**) Patella, (**b**) Achilles, (**c**) supraspinatus. Top row: haematoxylin and eosin. Bottom row: safranin O. T and B indicate tendon and bone tissues at their respective zone of the enthesis. Dashed squares indicate magnified areas. Scale bar = 100 μm.

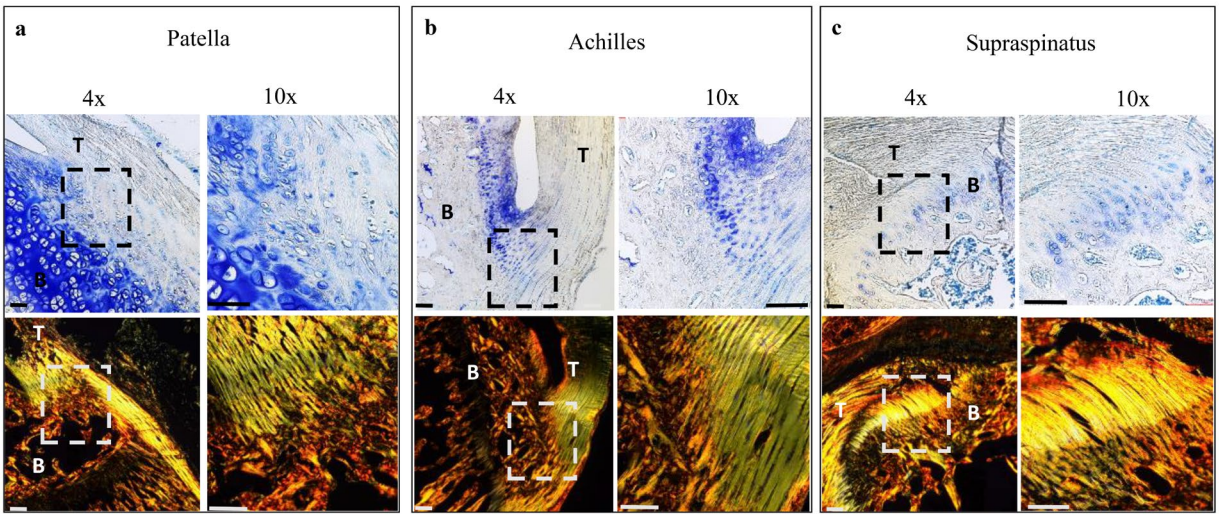


Fig. 4. Histological staining of native entheses. (**a**) Patella, (**b**) Achilles, (**c**) supraspinatus. Top row: toluidine blue. Bottom row: picrosirius red. T and B indicate tendon and bone tissues at their respective zone of the enthesis. Dashed squares indicate magnified areas. Scale bar = 100 μm.

Table 3. Orientation angle of the collagen fibres per location. [a] Values with no statistical difference from one another. [b] Values with statistical difference from the others ($p < 0.05$).

Enthesis	Orientation angle of the collagen fibres	Variation of orientation angle among ROIs
Achilles	41.14 ± 1.6	7.12 ± 2.24[a]
Patella	28.32 ± 5.25	3.19 ± 2.15[a]
Supraspinatus	56.00 ± 8.60	19.68 ± 5.28[b]

magnitude for the patellar and the Achilles entheses, which both had reported the longest tendons, whereas the supraspinatus, being the shortest tendon, resulted to be the weakest ($p < 0.001$). Conversely, the supraspinatus enthesis showed higher stiffness ($p < 0.001$) and higher tangent modulus whilst the patella and the Achilles were similar regarding both properties (Fig. 2**d**,**e**).

Histology

H&E, toluidine blue and safranin O stainings exposed differences in the morphology of the tendon-to-bone insertion site among the 3 locations (Fig. 3,4). The patellar enthesis exhibited a tendon-to-bone transition characterised by a proteoglycan-rich cartilaginous interphase between the tendon and the bony ends. The Achilles enthesis displayed a more abrupt transition from tendon to bone at the insertion site, while the supraspinatus presented a well-defined cartilage-like transition zone between the tendon and the bone.

The insertion angle of the collagen fibres from tendon to bone was determined using the picrosirius-red-stained sections (Table 3). The orientation angle measurements of the 3 ROIs for the Achilles and patellar entheses reported uniform values. The variation of the orientation angle among the ROIs of the patellar and the Achilles entheses showed no significant differences. However, the variation of the orientation angle among the ROIs of the supraspinatus was significantly higher than the variation measured in the patellar and the Achilles entheses ($p < 0.005$).

The IHC for the extracellular matrix collagens showed that, in the 3 instances, tendon and bone tissue were rich in collagen type I while the interface between these 2 tissues was positively stained for collagen type II. Interestingly, none of the 3 entheses showed visible deposition of collagen type III nor type X (Fig. 5).

Gene expression

The analysis of the gene expression from the 3 locations revealed significant differences among them (Fig. 6). The expression of *Col1a1* was significantly higher in the Achilles entheses samples than in the patellar and supraspinatus samples ($p < 0.005$ and $p < 0.05$, respectively), while the expression in the patellar entheses was not different from that of the supraspinatus. However, the expression of *Col2a1* was similar for the patellar and the Achilles entheses and, in both cases, higher than that measured in the supraspinatus samples ($p < 0.05$ and $p < 0.005$, respectively). Conversely, the expression of *Col3a1* was the highest in the supraspinatus entheses samples ($p < 0.001$) while the entheses samples from the Achilles and the patella showed very similar expression levels of *Col3a1*. Interestingly, *Col10a1* was not detected in the samples from the supraspinatus entheses and *Col10a1* expression in the Achilles and patellar entheses was similar and rather low.

In addition to the collagens, other tenogenic, chondrogenic and osteogenic markers were investigated (Fig. 6). The expression of *Mkx* and *Tnmd* was the highest in the Achilles samples ($p < 0.05$), while in the patella and the supraspinatus, these 2 genes were found to be expressed at similar, lower levels. In the same way, *Sox9*, *Runx2* and *Sparc* were highly expressed in the Achilles samples compared to the expression in the patella and supraspinatus entheses samples ($p < 0.05$). However, the expression of *Scx* was similar in the 3 locations while the expression of *Fn1* was the lowest in the patellar entheses samples, followed by the Achilles and reaching the highest levels of expression in the supraspinatus entheses samples ($p < 0.05$).

Discussion

The intricate biology of the tendon-to-bone enthesis has fascinated orthopaedics and tissue engineers for decades (Benjamin *et al.*, 1986; Lu and Thomopoulos, 2013; Schwartz *et al.*, 2012). The focus of most enthesis-related studies lies on either the patellar, the Achilles tendon or the supraspinatus enthesis (Baraliakos *et al.*, 2020; Lee *et al.*, 2017; Mattap *et al.*, 2018; Nawata *et al.*, 2002; Smietana *et al.*, 2017). A plausible explanation for that is the fact that these 3 entheses are among the more frequently injured ones (Apostolakos *et al.*, 2014). The present study aimed at a comparative characterisation of all these 3 insertion sites using different techniques in one study. Overall, the aim was to select the ultimate anatomical location for enthesis regeneration studies in the future.

Of the 3 analysed anatomical locations, the supraspinatus features the only intra-articular enthesis, while the patellar and Achilles' tendons entheses are of extra-articular nature (Derwin *et al.*, 2018). The intra-articular environment of the supraspinatus enthesis and its exposure to synovial fluid makes this insertion site an extraordinary challenging site for injury, susceptible to degenerative enthesopathies and acute trauma (Bedi *et al.*, 2009;

Derwin *et al.*, 2018; Yamamoto *et al.*, 2010). Hence, this explains the abundance of clinical reports addressing supraspinatus tears. However, with the biomechanical characterisation performed, it was observed the supraspinatus enthesis to be the smallest and weakest of the 3. Furthermore, the supraspinatus enthesis at the rotator cuff is rather cumbersome to access surgically, which is especially relevant when working with animal models of relatively small size (*e.g.* mice and rats). Besides, entheses regeneration studies usually involve the development of sponges and multiphasic scaffolds to provide a physical space for the new tissue to grow upon the creation of an enthesis defect (Font Tellado *et al.*, 2018; Wang *et al.*, 2021; Zhang *et al.*, 2018). Therefore, the small size and weakness of the supraspinatus enthesis of adult rats impose an additional challenge during the *in vivo* evaluation of such scaffolds at this location.

In the 3 investigated locations, the first zone of the enthesis (*i.e.* end of the tendon) was characterised by an arrangement of longitudinally aligned collagen type I bundles, clearly visible in the picrosirius red staining. This observation is in line with previous descriptions of the supraspinatus (Thomopoulos *et*

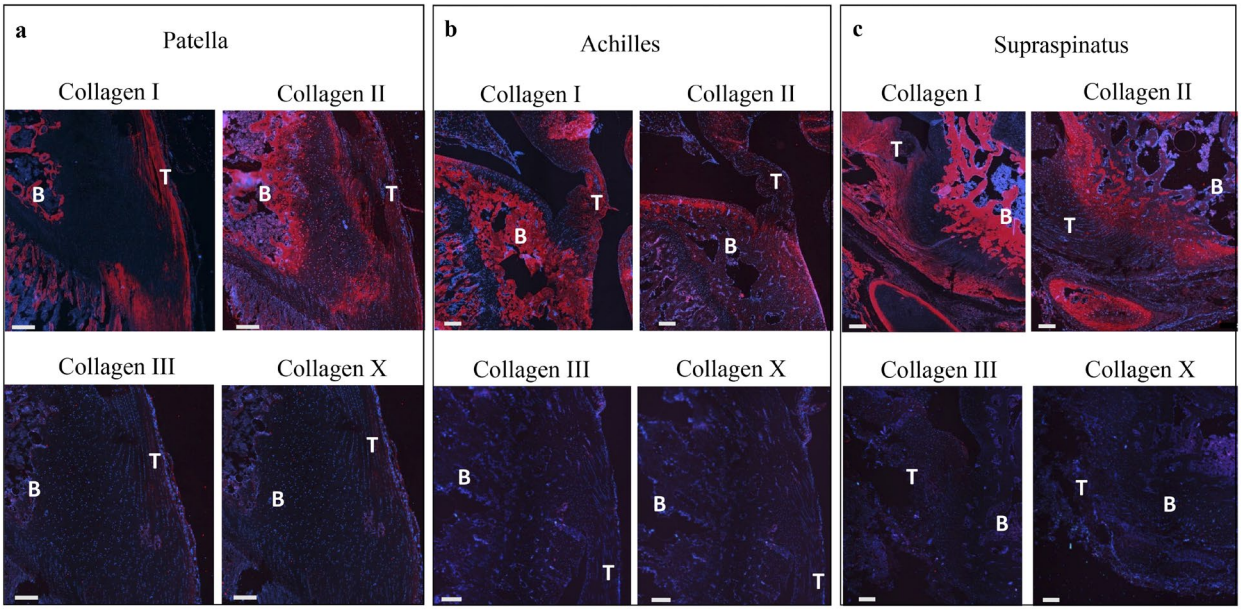


Fig. 5. Immunostaining of extracellular matrix collagens. Staining with Alexa Fluor 647 of the respective target antigen for each antibody. T and B indicate tendon and bone tissues at their respective sides of the enthesis. Counter staining with DAPI. Scale bar = 200 μm.

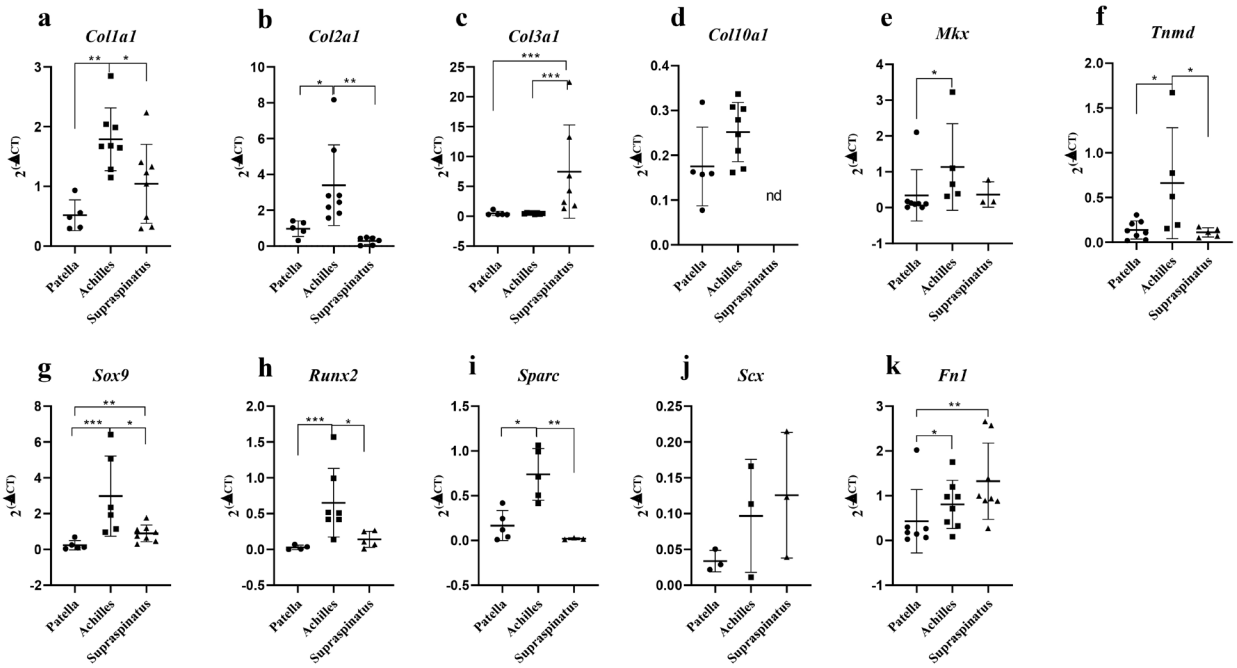


Fig. 6. Normalised gene expression at each location. (**a**) *Col1a1*, (**b**) *Col2a1*, (**c**) *Col3a1*, (**d**) *Col10a1*, (**e**) *Mkx*, (**f**) *Tnmd*, (**g**) *Sox9*, (**h**) *Runx2*, (**i**) *Sparc*, (**j**) *Scx* and (**k**) *Fn1*. Reference gene used for normalisation was β-tubulin. nd indicates non-detected, * $p < 0.05$, ** $p < 0.005$, *** $p < 0.001$. Lines indicate mean and standard deviation.

al., 2006), the Achilles tendon (Nourissat *et al.*, 2010; Sartori *et al.*, 2018) and the patellar tendon entheses (Domínguez *et al.*, 2017). Comparatively, the second zone of the enthesis, known as the fibrocartilaginous transition zone, was the less evident in the Achilles tendon enthesis, where the collagen bundles seem to connect more abruptly to the bone. However, the toluidine blue staining did show some positive staining for cartilage in the Achilles tendon enthesis, especially in the upper section of the tendon-to-bone interphase. A similar observation was done by Shaw *et al.* (2008) in samples of human Achilles entheses. In their study, they described a narrow fibrocartilaginous area more prominent in the superior part of the tendon-to-bone attachment as well as a sesamoid fibrocartilage zone in the section of the tendon immediately adjacent to the enthesis. This area is also visible in the safranin O staining of the deep section of the tendon, proximal to the calcaneus. Such zone, nearby the retro calcaneal bursa, is likely to be a high-stress concentration point where the friction between the tendon and the calcaneus yields a more chondrogenic phenotype (Amadio, 2005; Shaw *et al.*, 2008). Hence, the more cartilaginous appearance of the tissue in this area.

The transition from the second to the third zone of the enthesis was noticeably different between the patellar enthesis and the enthesis of the Achilles tendon and the supraspinatus. In the case of the patellar enthesis, the non-mineralised fibrocartilage area led to the large proteoglycan-rich zone of the tibial cartilage. This transition was similar in morphology to the proliferative and pre-hypertrophic zones observed in the growth plate of joints (Sun and Beier, 2014), where the chondrocytes are typically tightly packaged and arrange themselves into longitudinal columns. Liu *et al.* (2013) described a similar morphology of the patellar tendon insertion in mice. Such a large proteoglycan-rich area was not noticeable in the entheses of the supraspinatus and the Achilles tendons. Instead, in the supraspinatus enthesis, the aligned collagen bundles of the tendon were followed by a narrow fibrochondrogenic transition zone that abruptly connected to the trabecular bone. This morphology of the supraspinatus tendon enthesis was also described by Bedi *et al.* (2012) in mice. In the case of the Achilles tendon enthesis, the narrow rows of chondrocytes in between the collagen bundles connected the tendon directly to the perichondrium of the calcaneus. This was also observed in human samples of Achilles tendon entheses (Shaw *et al.*, 2008). Moreover, such a direct link has been described to be highly efficient in the dissipation of stress (Benjamin *et al.*, 2006). This is supported by the present study mechanical data since the Achilles enthesis showed the highest ultimate load per mm^2 among the 3 studied locations.

Interestingly and despite the observed histological differences at the insertion sites between the patellar enthesis and the Achilles tendon enthesis, these 2 locations showed comparable biomechanical properties. Both entheses were at least twice as strong and showed lower stiffness than the supraspinatus enthesis. Additionally, the variation of the orientation angle of the collagen fibres across the tendon-to-bone interphase of the Achilles and patellar enthesis was similar, while the supraspinatus showed a higher degree of variability of the orientation angle at the insertion site, which could contribute to the relatively poor performance of the supraspinatus enthesis during the tensile test. Furthermore, the insertion site of the patellar tendon displayed a cross-sectional area twice as big as that of the Achilles tendon and the supraspinatus entheses.

Up to this point, it is possible to argue that both the anatomy and biomechanical features of the rat patellar enthesis support the selection of this enthesis to be used as a model for enthesis regeneration studies. Nevertheless, it is worth pointing out that the ultimate load measured for the Achilles enthesis, if normalised to the enthesis cross-sectional area, is higher per mm^2 than that measured for the patellar entheses samples.

The histological analysis confirmed the presence of type I collagen-rich tendons that were inserted into the bone through a type II collagen-rich transition zone for all the 3 entheses studied. Yet, no noticeable deposition of collagen type III nor type X was observed in any of the 3 locations studied. This observation was partially in line with that of Dyment *et al.* (2015). In their work, the authors compared the deposition of collagen type I, II and X in the patellar tendon, supraspinatus tendon and Achilles tendon entheses at different maturation stages (*i.e.* postnatal day 1, 2 weeks and 4 weeks). They observed similar patterns of collagen type I deposition to that described in the present work. However, after 4 weeks of entheses maturation, they did not observe collagen type II expression at the enthesial interphase. Interestingly, the authors reported deposition of collagen type X within the mineralised fibrocartilage (Dyment *et al.*, 2015).

The gene expression data provided crucial insights in the collagen expression of the 3 locations. On the one hand, the highest *Col1a1* expression was measured in the Achilles enthesis samples. Collagen type I is the major component of the extracellular matrix of the tendons and is, for the most part, responsible for the mechanical properties of this tissue (Buckley *et al.*, 2013; Franchi *et al.*, 2007). The elevated expression of *Col1a1* in the Achilles samples might explain the high ultimate load measured for this enthesis, which was comparable to that of the patellar enthesis, while showing a fraction of the patellar tendon's cross-sectional area. On the other hand, the expression of *Col3a1* was the highest in the supraspinatus enthesis, which, displaying a similar cross-sectional area to that of the Achilles enthesis, performed poorly in the biomechanical test. In healthy tendons, collagen type III fibrils are associated with collagen type I (Buckley *et al.*, 2013). However, disorganisation and random orientation of

the collagen type III fibres typically yields a weaker structure than collagen type I. The ratio of collagen type III/I increases with ageing and the presence of pathologies (Gonçalves-Neto *et al.*, 2002; Smith *et al.*, 1999).

The expression of the transcription factor *Mkx* was the highest in the Achilles enthesis. This observation goes in line with the *Col1a1* expression pattern previously described since *Mkx* acts as a positive regulator of collagen type I expression (Ito *et al.*, 2010). In a similar way, the higher expression of *Sox9* in the Achilles entheses samples could cause the high expression of *Col2a1* in these samples, since the expression of collagen type II by chondrocytes at the enthesis is activated by the transcription factor *Sox9* (Eames *et al.*, 2004). Interestingly, the expression of *Col2a1* in the patellar enthesis was similar to that of the Achilles enthesis while the expression of *Sox9* measured in the patellar samples was the lowest of the 3. However, the higher expression of *Col2a1* in the patellar tendon and the Achilles tendon entheses compared to the supraspinatus entheses could be related to the higher compressive loads at which the patellar tendon and Achilles entheses are exposed due to their anatomical location (Docking *et al.*, 2013; Franchi *et al.*, 2007). Nevertheless, the tendon-to-bone transition zone of the 3 analysed entheses stained positive for collagen type II.

The expression of *Scx* was low in the 3 locations and only 3 samples per group showed expression values high enough to render Ct values lower than the cut-off value of 35. However, such low expression of *Scx* was expected in the entheses samples since this early marker of tenogenesis is usually expressed in tendons during the stages of organogenesis or at the early stages of healing (Murchison *et al.*, 2007; Shukunami *et al.*, 2018).

Overall, each of the 3 entheses showed a very distinctive pattern of gene expression. On the one hand, samples from the Achilles enthesis consistently showed higher levels of expression of chondrogenic, osteogenic and tenogenic markers than the other 2 locations. On the other hand, the expression of chondrogenic markers in the supraspinatus enthesis samples was relatively higher than in the patellar tendon entheses. The observed differences between the 3 analysed entheses illustrated how anatomical location and function dictate the mechanical properties, morphology and local gene expression. Additionally, the present study demonstrated that the 3 entheses were essentially different, thus, a unique model to study enthesis, as an organ, might not always be suitable. This is, undeniably, one major limitation that tissue engineers face when studying tendon-to-bone entheses, especially in small animal models. The gained insight into such differences facilitates the translation of pre-clinical investigation for specific enthesis injury sites. However, there are practical limitations to this study associated with the challenge of working with interphase tissues from small-animal models. Ensuring a clean preparation of the enthesis is difficult. For the present study, a single/same operator performed all the sample preparation to ensure consistency. This procedure was extensively rehearsed. The measurements of the entheses and tendons were performed by the same operator utilising high-accuracy equipment to conduct all measurements. Cross-sectional areas were assumed to be rectangular in nature and, thus, allowed standardisation and assessment across the samples from each anatomical location. This assumption was a limitation; however, the authors do not believe that higher accuracy assessments were practically feasible. Ultimately, the patellar samples showed the highest reported cross-sectional areas and, thus, expected higher failure loads corroborating the measurements.

Conclusion

The comparative characterisation performed in the present study provided valuable insights for a better understanding of 3 entheses at relevant anatomical sites. To the best of the authors' knowledge, such a direct comparison of entheses tissues corresponding to 3 different anatomical locations has not been reported before. On the one hand, the gene expression analysis allowed to compare the expression patterns of genes important for the healing of tendon, cartilage and bone tissue at the 3 investigated locations. On the other hand, biomechanical evaluations revealed that the patellar tendon enthesis and the Achilles enthesis featured the highest ultimate load resistance combined with the lowest stiffness. However, the large cross-sectional area of the patellar tendon at the enthesis and the convenient surgical accessibility to the patellar region, allowed the authors to conclude that the patellar tendon enthesis site would be most suitable for the development of a preclinical model for general enthesis regeneration studies in rats.

Acknowledgments

This study has been partially funded by the ON Kick Starter Grant (project number 20-105). Dr Evans's research is partly funded by the John and Posy Krehbiel Professorship in Orthopedics. This work was supported by the Province of Limburg, Limburg Invests in its Knowledge Economy (LINK).

The authors declare that there are no competing interests.

References

Amadio PC (2005) Friction of the gliding surface. Implications for tendon surgery and rehabilitation. J Hand Ther **18**: 112-119.

Apostolakos J, Durant TJ, Dwyer CR, Russell RP, Weinreb JH, Alaee F, Beitzel K, McCarthy MB, Cote

MP, Mazzocca AD (2014) The enthesis: a review of the tendon-to-bone insertion. Muscles Ligaments Tendons **4**: 333-342.

Baraliakos X, Sewerin P, de Miguel E, Pournara E, Kleinmond C, Wiedon A, Behrens F (2020) Achilles tendon enthesitis evaluated by MRI assessments in patients with axial spondyloarthritis and psoriatic arthritis: a report of the methodology of the ACHILLES trial. BMC Musculoskelet Disord **21**: 767. DOI: 10.1186/s12891-020-03775-4.

Baumans V (2004) Use of animals in experimental research: an ethical dilemma? Gene Therapy **11**: S64-S66.

Bedi A, Kawamura S, Ying L, Rodeo SA (2009) Differences in tendon graft healing between the intra-articular and extra-articular ends of a bone tunnel. HSS J **5**: 51-57.

Bedi A, Maak T, Walsh C, Rodeo SA, Grande D, Dines DM, Dines JS (2012) Cytokines in rotator cuff degeneration and repair.J Shoulder Elbow Surg **21**: 218-227.

Benjamin M, Bollow M, Brandt JAN, Braun J, Burgos-Vargas R, Claudepierre P, De Vlam K, Eulderink F, Fassbender H-G, Fitzgerald O, François R, Häupl T, Heinegard D, Khan MA, Kriegsmann J, Leirisalo-Repo M, McGonagle D, Olivieri I, Sieper J, Zhang Y, Braun J, Braun J, Sieper J, Veys E, Sittinger M, Gay S, Braun J, Poole AR (2000) Anatomy and biochemistry of entheses. Ann Rheum Dis **59**: 995. DOI: 10.1136/ard.59.12.995.

Benjamin M, Evans EJ, Copp L (1986) The histology of tendon attachments to bone in man. J Anat **149**: 89-100.

Benjamin M, Kumai T, Milz S, Boszczyk BM, Boszczyk AA, Ralphs JR (2002) The skeletal attachment of tendons—tendon 'entheses'. Comp Biochem Physiol A Mol Integr Physiol **133**: 931-945.

Benjamin M, Toumi H, Ralphs JR, Bydder G, Best TM, Milz S (2006) Where tendons and ligaments meet bone: attachment sites ('entheses') in relation to exercise and/or mechanical load. J Anat **208**: 471-490.

Buckley MR, Evans EB, Matuszewski PE, Chen Y-L, Satchel LN, Elliott DM, Soslowsky LJ, Dodge GR (2013) Distributions of types I, II and III collagen by region in the human supraspinatus tendon. Connect Tissue Res **54**: 374-379.

Bunker DL, Ilie V, Ilie V, Nicklin S (2014) Tendon to bone healing and its implications for surgery. Muscles Ligaments Tendons J **4**: 343-350.

Calejo I, Costa-Almeida R, Reis RL, Gomes ME (2019) Enthesis tissue engineering: biological requirements meet at the interface. Tissue Eng Part B Rev **25**: 330-356.

Derwin KA, Galatz LM, Ratcliffe A, Thomopoulos S (2018) Enthesis repair: challenges and opportunities for effective tendon-to-bone healing. J Bone Joint Surg Am **100**: e109-e109.

Docking S, Samiric T, Scase E, Purdam C, Cook J (2013) Relationship between compressive loading and ECM changes in tendons. Muscles Ligaments Tendons J **3**: 7-11.

Domínguez D, Contreras-Muñoz P, Lope S, Rodas G, Marotta M (2017) Generation of a new model of patellar tendinopathy in rats which mimics the human sports pathology: a pilot study. Apunts **52**: 53-59.

Dyment NA, Breidenbach AP, Schwartz AG, Russell RP, Aschbacher-Smith L, Liu H, Hagiwara Y, Jiang R, Thomopoulos S, Butler DL, Rowe DW (2015) Gdf5 progenitors give rise to fibrocartilage cells that mineralize *via* hedgehog signaling to form the zonal enthesis. Dev Biol **405**: 96-107.

Eames BF, Sharpe PT, Helms JA (2004) Hierarchy revealed in the specification of three skeletal fates by Sox9 and Runx2. Dev Biol **274**: 188-200.

Fan L, Xu B, Liu N, Wang L (2020) Histopathological changes in patellar tendon enthesis of rabbit induced by electrical stimulation intensity. J Orthop Sci **25**: 344-348.

Font Tellado S, Bonani W, Balmayor ER, Foehr P, Motta A, Migliaresi C, van Griensven M (2017) Fabrication and characterization of biphasic silk fibroin scaffolds for tendon/ligament-to-bone tissue engineering. Tissue Eng Part A **23**: 859-872.

Font Tellado S, Chiera S, Bonani W, Poh PSP, Migliaresi C, Motta A, Balmayor ER, van Griensven M (2018) Heparin functionalization increases retention of TGF-β2 and GDF5 on biphasic silk fibroin scaffolds for tendon/ligament-to-bone tissue engineering. Acta Biomater **72**: 150-166.

Franchi M, Trirè A, Quaranta M, Orsini E, Ottani V (2007) Collagen structure of tendon relates to function. ScientificWorldJournal **7**: 404-420.

Fu S-C, Yeung M-Y, Rolf CG, Yung PS-H, Chan K-M, Hung L-K (2018) Hydrogen peroxide induced tendinopathic changes in a rat model of patellar tendon injury. J Orthop Res **36**: 3268-3274.

Gonçalves-Neto J, Witzel SS, Teodoro WR, Carvalho-Junior AE, Fernandes TD, Yoshinari HH (2002) Changes in collagen matrix composition in human posterior tibial tendon dysfunction. Joint Bone Spine **69**: 189-194.

Holwein C, von Bibra B, Jungmann PM, Karampinos DC, Wörtler K, Scheibel M, Imhoff AB, Buchmann S (2019) No healing improvement after rotator cuff reconstruction augmented with an autologous periosteal flap. Knee Surg Sports Traumatol Arthrosc **27**: 3212-3221.

Ito Y, Toriuchi N, Yoshitaka T, Ueno-Kudoh H, Sato T, Yokoyama S, Nishida K, Akimoto T, Takahashi M, Miyaki S, Asahara H (2010) The Mohawk homeobox gene is a critical regulator of tendon differentiation. Proc Natl Acad Sci U S A **107**: 10538-10542.

Killian ML (2021) Growth and mechanobiology of the tendon-bone enthesis. Semin Cell Dev Biol **23**: 64-73.

Lee KW, Lee JS, Kim YS, Shim YB, Jang JW, Lee KI (2017) Effective healing of chronic rotator cuff injury using recombinant bone morphogenetic protein-2 coated dermal patch *in vivo*. J Biomed Mater Res B Appl Biomater **105**: 1840-1846.

Liu C-F, Breidenbach A, Aschbacher-Smith L, Butler D, Wylie C (2013) A role for hedgehog signaling in the differentiation of the insertion site of the patellar tendon in the mouse. PloS One **8**: e65411. DOI: 10.1371/journal.pone.0065411.

Lu HH, Thomopoulos S (2013) Functional attachment of soft tissues to bone: development, healing, and tissue engineering. Annu Rev Biomed Eng **15**: 201-226.

Mattap S, Aitken D, Wills K, Halliday A, Ding C, Han W, Cicuttini F, Jones G, Laslett L (2018) Patellar tendon enthesis abnormalities and their association with knee pain and structural abnormalities in older adults. Osteoarthritis Cartilage **26**: S412-S413.

Murchison ND, Price BA, Conner DA, Keene DR, Olson EN, Tabin CJ, Schweitzer R (2007) Regulation of tendon differentiation by scleraxis distinguishes force-transmitting tendons from muscle-anchoring tendons. Development **134**: 2697-2708.

Nawata K, Minamizaki T, Yamashita Y, Yamashita Y, Teshima R, Teshima R (2002) Development of the attachment zones in the rat anterior cruciate ligament: changes in the distributions of proliferating cells and fibrillar collagens during postnatal growth. J Orthop Res **20**: 1339-1344.

Nourissat G, Diop A, Maurel N, Salvat C, Dumont S, Pigenet A, Gosset M, Houard X, Berenbaum F (2010) Mesenchymal stem cell therapy regenerates the native bone-tendon junction after surgical repair in a degenerative rat model. PloS One **5**: e12248. DOI: 10.1371/journal.pone.0012248.

Novakova SS, Mahalingam VD, Florida SE, Mendias CL, Allen A, Arruda EM, Bedi A, Larkin LM (2018) Tissue-engineered tendon constructs for rotator cuff repair in sheep. J Orthop Res **36**: 289-299.

Nowlin J, Bismi MA, Delpech B, Dumas P, Zhou Y, Tan GZ (2018) Engineering the hard-soft tissue interface with random-to-aligned nanofiber scaffolds. Nanobiomedicine **5**: 1849543518803538. DOI: 10.1177/1849543518803538.

Paxton J, Baar K, Grover L (2012) Current progress in enthesis repair: strategies for interfacial tissue engineering. Orthopedic Muscul Sys. DOI: 10.4172/2161-0533.S1-003.

Quirk NP, Lopez De Padilla C, De La Vega RE, Coenen MJ, Tovar A, Evans CH, Müller SA (2018) Effects of freeze-thaw on the biomechanical and structural properties of the rat Achilles tendon. J Biomech **81**: 52-57.

Rossetti L, Kuntz LA, Kunold E, Schock J, Muller KW, Grabmayr H, Stolberg-Stolberg J, Pfeiffer F, Sieber SA, Burgkart R, Bausch AR (2017) The microstructure and micromechanics of the tendon-bone insertion. Nat Mater **16**: 664-670.

Rothrauff BB, Smith CA, Ferrer GA, Novaretti JV, Pauyo T, Chao T, Hirsch D, Beaudry MF, Herbst E, Tuan RS, Debski RE, Musahl V (2019) The effect of adipose-derived stem cells on enthesis healing after repair of acute and chronic massive rotator cuff tears in rats.J Shoulder Elbow Surg **28**: 654-664.

Sartori J, Köhring S, Witte H, Fischer MS, Löffler M (2018) Three-dimensional imaging of the fibrous microstructure of Achilles tendon entheses in *Mus musculus*. J Anat **233**: 370-380.

Schwartz AG, Pasteris JD, Genin GM, Daulton TL, Thomopoulos S (2012) Mineral distributions at the developing tendon enthesis. PloS One **7**: e48630-e48630. DOI: 10.1371/journal.pone.0048630.

Shaw HM, Vázquez OT, McGonagle D, Bydder G, Santer RM, Benjamin M (2008) Development of the human Achilles tendon enthesis organ. J Anat **213**: 718-724.

Shukunami C, Takimoto A, Nishizaki Y, Yoshimoto Y, Tanaka S, Miura S, Watanabe H, Sakuma T, Yamamoto T, Kondoh G, Hiraki Y (2018) Scleraxis is a transcriptional activator that regulates the expression of tenomodulin, a marker of mature tenocytes and ligamentocytes. Sci Rep **8**: 3155. DOI: 10.1038/s41598-018-21194-3.

Silver N, Best S, Jiang J, Thein SL (2006) Selection of housekeeping genes for gene expression studies in human reticulocytes using real-time PCR. BMC Mol Biol **7**: 33-33.

Smietana MJ, Moncada-Larrotiz P, Arruda EM, Bedi A, Larkin LM (2017) Tissue-engineered tendon for enthesis regeneration in a rat rotator cuff model. Biores Open Access **6**: 47-57.

Smith RK, Birch H, Patterson-Kane J, Firth EC, Williams L, Cherdchutham W, Weeren WRv, Goodship AE (1999) Should equine athletes commence training during skeletal development?: changes in tendon matrix associated with development, ageing, function and exercise. Equine Vet J Suppl **31**: 201-209.

Su W, Wang Z, Jiang J, Liu X, Zhao J, Zhang Z (2019) Promoting tendon to bone integration using graphene oxide-doped electrospun poly(lactic-co-glycolic acid) nanofibrous membrane. International journal of nanomedicine **14**: 1835-1847.

Sun MM-G, Beier F (2014) Chondrocyte hypertrophy in skeletal development, growth, and disease. Birth Defects Res C Embryo Today **102**: 74-82.

Sun Y, Kwak J-M, Kholinne E, Zhou Y, Tan J, Koh KH, Jeon I-H (2020) Small subchondral drill holes improve marrow stimulation of rotator cuff repair in a rabbit model of chronic rotator cuff tear. Am J Sports Med **48**: 706-714.

Thomopoulos S, Marquez JP, Weinberger B, Birman V, Genin GM (2006) Collagen fiber orientation at the tendon to bone insertion and its influence on stress concentrations. J Biomech **39**: 1842-1851.

Wang W, Qin S, He P, Mao W, Chen L, Hua X, Zhang J, Xiong X, Liu Z, Wang P, Meng Q, Dong F, Li A, Chen H, Xu J (2021) Type II collagen sponges facilitate tendon stem/progenitor cells to adopt more chondrogenic phenotypes and promote the regeneration of fibrocartilage-like tissues in a rabbit partial patellectomy model. Front Cell Dev Biol **9**: 1805. DOI: 10.3389/fcell.2021.682719.

Watad A, Cuthbert RJ, Amital H, McGonagle D (2018) Enthesitis: much more than focal insertion

point inflammation. Curr Rheumatol Rep **20**: 41. DOI: 10.1007/s11926-018-0751-3.

Wieloch P, Buchmann G, Roth W, Rickert M (2004) A cryo-jaw designed for *in vitro* tensile testing of the healing Achilles tendons in rats. J Biomech **37**: 1719-1722.

Yamamoto A, Takagishi K, Osawa T, Yanagawa T, Nakajima D, Shitara H, Kobayashi T (2010) Prevalence and risk factors of a rotator cuff tear in the general population.J Shoulder Elbow Surg **19**: 116-120.

Zhang J, Nie D, Zhao G, Tan S, Hogan M, Wang J (2018) A Novel kartogenin-releasing polymer scaffold promotes wounded rat achilles tendon enthesis healing. Foot & Ankle Orthopaedics **3**: 2473011418S2473000532. DOI: 10.1177/2473011418S00532.

Zhao F, Lacroix D, Ito K, van Rietbergen B, Hofmann S (2020) Changes in scaffold porosity during bone tissue engineering in perfusion bioreactors considerably affect cellular mechanical stimulation for mineralization. Bone Rep **12**: 100265. DOI: 10.1016/j.bonr.2020.100265.

Discussion with Reviewers

Andreas Traweger: The pathogenesis, mechanical loading and chronicity are arguably different between small animal models and humans, ultimately limiting the translational value of these models. As the authors propose the rat patellar enthesis defect model as a favourable one to develop novel strategies for enthesis repair, which outcome factors would the authors suggest are of greatest value for determining the benefit of *e.g.* a novel biomaterial? How meaningful are the results from biomechanical testing without a standardised testing procedure used by most laboratories? Should researchers be focusing on structural repair as evidenced by histology, immunohistochemistry, molecular analysis *etc.*? In other words, is the greatest value of small animal models mostly (only) to demonstrate biocompatibility of a newly developed biomaterial?
Authors: We agree with the reviewer that the translational value of small animal models is limited by fundamental differences between such models and humans (*i.e.* size, weight, anatomy, physiology, *etc.*). However, in our view, the use of small animal models has still plenty to offer in the pursuit of answering to novel scientific questions other than solely demonstrating biocompatibility of a given biomaterial. Such small-animal models represent a valuable platform for the proof of concepts of novel therapies or ideas for which cell models are far less suitable, without incurring in the high costs and complex logistics associated with the handling, care and use of large-animal models. That been said, it is up to the researchers from biomedical fields to optimise the way small-animal models are used to ensure getting the right answers to the right questions.

Regarding which outcome factors should be used to determine the benefits of *e.g.* a novel biomaterial, we believe that, at least in musculoskeletal research, the restoration of functionality as well as a similar histology/molecular biological footprint of the treated limb/organ/joint to their native parameters after injury, could act as a fairly good indicator of the effectiveness of the biomaterial/therapy used.

Reviewer: I agree that an easy surgical approach might be important for a pre-clinical model. However, the *in vivo* mechanics might also affect the healing and might not be comparable between the 3 enthesis and thereby affecting healing. Can the authors comment on this?
Authors: As the reviewer pointed out, the differences of the *in vivo* mechanics might affect healing. This is an important aspect to consider when aiming to compare the healing process of the three entheses. However, it is not the only aspect that might make such comparison difficult. The present study characterised three different healthy entheses and found differences in the morphology of the attachment site and in their molecular environment, all of which could also influence the healing process upon injury. A pre-clinical model was proposed that offers an easier surgical approach to one of the three most relevant sites of entheses injury. Nevertheless, by characterising and listing fundamental differences between the three entheses, we are paving the way to equalising the differences of healing outcome for potential therapies developed using such pre-clinical model when applied to other entheses.

Editor's note: The Guest Editor responsible for this paper was Manuela Gomes.